

Effect of graphene oxide on the properties of compatibilized polypropylene/ethylene-propylene-rubber blend

Zahir Guezout¹ · Rachida Doufnoune¹ · Nacerddine Haddaoui²

Received: 29 March 2017 / Accepted: 24 July 2017
© Springer Science+Business Media B.V. 2017

Abstract In this work, the effect of graphene oxide (GO) and its derivatives on the mechanical, thermal and morphological properties of nanocomposites based on polypropylene/ethylene-propylene rubber (PP/EPR) were investigated. In order to achieve a better dispersion of the nanofiller and to enhance its interaction with the polymer matrix, amine and alcohol grafted polypropylene were used as compatibilizers. These compatibilizers were synthesized by the reaction of polypropylene-grafted anhydride maleic (PP-g-MAH) with 1,12-dodecanediamine and 1,12-dodecanediol, respectively in the presence of dicumyl peroxide (DCP) by melt mixing. The nanocomposites were prepared via melt blending masterbatch process using Brabender mixer. The addition of functionalized GO and compatibilizers improved the tensile strength and Young's modulus of PP/EPR nanocomposite. While the elongation and Izod impact strength were adversely affected. Furthermore, the TGA analysis showed that the incorporation of GO and compatibilizers improve significantly the thermal stability. SEM micrographs of the fractured surfaces of the nanocomposites revealed a good dispersion of functionalized GO in the polymer matrix.

Keywords PP · EPR · Graphene oxide · Intercalation · Coupling agents · Nanocomposites

✉ Rachida Doufnoune
doufnoune@yahoo.fr

¹ Unité de Recherche sur les Matériaux Emergents –Sétif- URMES, Equipe de Valorisation des Polymères, Université Ferhat ABBAS Sétif-1, Sétif, Algérie

² Laboratoire de Physico-Chimie des Hauts Polymères (LPCHP), Département de Génie des Procédés, Faculté de Technologie, Université Ferhat ABBAS Sétif-1, Sétif, Algérie

Introduction

Over the last few decades, interest in a new class of carbon-based nanomaterials, such as carbon nanotubes (CNTs) and fullerene have rapidly gained more attention as nanofillers for polymer nanocomposites. This is due to their potential for improving physical and structural properties compared to conventionally carbon black filled polymers [1, 2].

Graphene is the most recent addition to members of the carbon family. As the building blocks for CNTs and other carbon nanomaterials, graphene structure consists of a flat monolayer of sp²-hybridized carbon atoms, hexagonally arrayed. This unique structure provides this material with exceptional properties, in particular high ultimate strength (130 GPa) and Young's modulus (1TPa). In addition, graphene also have high specific surface area of 2630–2965 m²/g, high aspect ratio and low mass density. The dispersion of small quantity of such materials in polymer matrices produces nanocomposites with superior mechanical properties [3, 4]. However, nowadays, there are still some big technical challenges, e.g., high cost of manufacturing pure monolayer graphene. Moreover, due to its strong van der Waals interactions and high specific surface area, it is very difficult to disperse a large quantity of graphene into polymer matrices. While the graphene oxide (GO), consisting of graphene derived sheets and other oxygen functional groups are showing more potential for practical applications [5].

GO can be produced by the oxidation and exfoliation of graphite with strong oxidative reagents such as HNO₃, H₂SO₄, H₂O₂, KMnO₄, KClO₃, NaNO₃ ... [6]. GO consists of oxygen functional groups on the basal plane and at the edges. In the majority of cases, it is believed that epoxy and hydroxyl groups are on the basal plane, whereas carbonyl and carboxylic acid groups are at the edges [6, 7]. The functionalities on the surface of GO can promote complete exfoliation of

graphene oxide sheets in polymeric matrices and enhance the interfacial interaction notably [5, 8].

GO has been employed in many polymer matrix-nanocomposites (PNCs) because it has a potentially effective reinforcement. However, GO is highly hydrophilic and most engineering polymers are hydrophobic. The dispersion of GO in most cases is not easily achieved due to the intrinsic incompatibility of GO and engineering polymers [9, 10]. In order to have a successful development of PNCs, it is necessary to modify GO so that it can be compatible with a given polymer matrix.

Because the rich chemistry of hydroxyl, carboxyl, and epoxy groups, GO has been selected very often as the starting material for the formation of GO derivatives through the covalent organic groups grafted on its surface [6, 11]. Numerous GO derivatives can be obtained based on the reaction with epoxy and carboxylic acid groups on GO sheets. Nucleophilic substitution, acylation and esterification are frequently used as approaches to modify GO. Yuan [12] employed *p*-phenylenediamine (PPD) for the modification of GO through the reaction with epoxy groups generating GO-PPD. Then, GO-PPD is modified with cyanuric chloride (CC) and grafted with maleic anhydride-*g*-polypropylene to produce functionalized GO/PP (fGO/PP) nanocomposites. It has been shown that the conductivity, thermal stability and mechanical properties of the nanocomposites are enhanced effectively by the addition of fGO.

Ren et al. [13] reported a method to efficiently convert the hydrophilic groups of GO and reduced graphene oxide (RGO) into alkyl groups by nucleophilic substitution and amidation reaction with dodecylamine (DA). The resulting functionalized nanomaterials (DA-GO) and (DA-RGO) can be homogeneously dispersed in high density-polyethylene (HDPE). The crystallinity, dynamic mechanical, gas barrier, and thermal stability properties of HDPE were greatly enhanced by the addition of a low concentration of DA-GO or DA-RGO.

Polyolefin nanocomposites based on GO nanosheets offer opportunities for the improvement of polyolefins (POs) with relatively small amounts of nanofiller concentration [14–17]. PP is the polymer that probably offers the best price/performance ratio among all POs. With a tonnage representing over 21% of total plastics it is estimated to have an average annual growth rate of 4% for the period from 2010 to 2020 [18]. This is one of the most widely used materials after polyethylene, polystyrene and polyvinyl chloride. It is used for large automotive exterior applications requiring durability, and ductile impact properties at low temperature. Applications include bumpers and other large exterior parts due to its low density, easy processing, thermal stability, resistance to corrosion and good resistance to impact [19].

Polypropylene is often produced and marketed in the form of PP/elastomer compounds such as PP/EPR (ethylene-propylene rubber), PP/EPDM (ethylene-propylene-diene monomer) and PP/POE (polyethylene-octene) blends. They are characterized

by an increased impact resistance in a wide temperature range from ambient to -40 °C. However, their use is limited when the thermo-mechanical properties combined with high stiffness and temperature resistance are required. It appears desirable to combine the advantages of the two systems and to elaborate ternary nanocomposites, which contain both an elastomer and nanofiller [20, 21]. However, the main challenge in the fabrication of nanocomposites is dispersion of the individual GO nanosheets in the polymer blends, due to the incompatibility of hydrophobic matrix with hydrophilic GO. Therefore, surface modifications of the GO nanoparticles and the addition of functional compatibilizers are often required to achieve the intercalation and exfoliation morphologies necessary for reaching the best mechanical performances.

The main objective of this paper is to examine the effect of GO nanoparticles and compatibilizers on the properties of PP/EPR/GO nanocomposites prepared by melt compounding mixing process (masterbatch dilution technique) using Brabender mixer. The influences of GO loading and surface modifications of GO with hexadecylamine and silane coupling agents on the mechanical, thermal and structural properties of the nanocomposites were investigated.

Experimental

Materials

The materials used in this work are presented in Table 1. Natural graphite powder particles (10 μm) were supplied from Qingdao Xinghe Graphite co. Ltd., China. The chemicals used for the synthesis of graphene oxide, sulfuric acid (H₂SO₄, 98%), fumed nitric acid (HNO₃, 68%), hydrogen peroxide (H₂O₂, 30%), and hydrofluoric acid (HF, 48%) were obtained from Sigma-Aldrich without any further purification. Hexadecylamine (HDA, 98%) was supplied from Fluka. γ -glycidoxytrimethoxysilane (GPTMS, > 98%) was purchased from Sigma-Aldrich and γ -aminopropyltriethoxysilane (AMPTES, > 99%) was generously donated by Witco Corp. (USA). The chemical formulas of the silane coupling agents are presented in Fig. 1. The polypropylene (ISPLEN PP040 G1E) used as the matrix is an isotactic homopolymer obtained from Repsol Quimica S.A. (Spain). The Ethylene-Propylene Rubber (EPR) employed in this study is a commercial grade product (Vistalon) from Exxon Mobil Chemical. The ethylene/propylene ratio of this material is 70/30. Maleic anhydride (MAH, 99%) and dicumyl peroxide (DCP, 98%) were supplied from Sigma-Aldrich. The diamine (1,12-dodecanediamine, 99%) and dialcohol (1,12-dodecanediol 99%) purchased from Sigma-Aldrich were used to functionalize PP. All other reagents which were laboratory grade and supplied from Sigma-Aldrich were

Table 1 Materials used in this study

Materials	Commercial designation	Supplier	Properties
Graphite	Natural graphite	Qingdao Xinghe Graphite co. Ltd	$d_{50} = 10 \mu\text{m}$
PP	ISPLEN PP040 G1E	Repsol Quimica S.A.	$\text{MFI} = 3 \text{ g}/10 \text{ min}$, $d = 0.902 \text{ g}/\text{cm}^3$
EPR	Vistalon	Exxon Mobil Chemical	$M_L (1 + 4) = 30$ at $125 \text{ }^\circ\text{C}$, $d = 0.88 \text{ g}/\text{cm}^3$
MAH	Maleic anhydride	Sigma-Aldrich	$\text{bp} = 202 \text{ }^\circ\text{C}$, $d = 1.48 \text{ g}/\text{cm}^3$
DCP	Dicumyl peroxide	Sigma-Aldrich	$\text{bp} = 31\text{-}^\circ\text{C}$, $d = 1.56 \text{ g}/\text{cm}^3$
ODA	n-Octadecylamine	Fluka	$\text{bp} = 232 \text{ }^\circ\text{C}$, $\text{mp} = 52 \text{ }^\circ\text{C}$
GPTMS	GLYMO	Sigma-Aldrich	$d = 1.069 \text{ g}/\text{cm}^3$, $\text{bp} = 120 \text{ }^\circ\text{C}$
AMPTES	Silquest A-1100	Witco Corp.	$d = 0.95 \text{ g}/\text{cm}^3$, $\text{bp} = 92 \text{ }^\circ\text{C}$
Diamine	1,12-dodecanediamine	Sigma-Aldrich	$\text{bp} = 67 \text{ }^\circ\text{C}$
Dialcohol	1,12-dodecanediol	Sigma-Aldrich	$\text{bp} = 79 \text{ }^\circ\text{C}$

used without further purification unless otherwise specified. The maleic, amine and alcohol functionalized compatibilizers were prepared in our laboratory.

Synthesis of graphene oxide

The natural graphite was first purified following two consecutive steps: an oxidative treatment in air at $350 \text{ }^\circ\text{C}$ for 30 min followed by a chemical one using a mixed aqueous solution containing 30 wt% of hydrogen peroxide and 30 wt% of hydrofluoric acid at a temperature of $80 \text{ }^\circ\text{C}$.

GO powders were prepared via a chemical approach according to the following procedure: 10 g of purified powder graphite was dispersed in a mixture of concentrated sulfuric acid and fuming nitric acid in a ratio of 60:40. The obtained mixture was refluxed under vigorous stirring for 72 h. Afterwards, 200 ml of distilled water was added to the reaction vessel. The diluted slurry was then stirred for an additional 5 h. The product was filtered and washed with distilled water in order to remove the impurities. The resulting GO

was then dried in a vacuum oven at $65 \text{ }^\circ\text{C}$ for 36 h and then grinded in fine particles.

Intercalation and functionalization of graphene oxide

Intercalation of GO with octadecylamine was performed by the following procedure: Typically, 6 g of octadecylamine was dissolved in 100 ml ethanol and added dropwise to a suspension of 2 g of GO in 300 ml of water under vigorous stirring. The reaction lasted for 24 h at $80 \text{ }^\circ\text{C}$ and the intercalated GO was collected by filtration and thoroughly washed with 25:75 warm water/ethanol mixtures three times. The obtained product was filtered then dried at $60 \text{ }^\circ\text{C}$ for 72 h prior to characterization. The modified GO which was ground to fine particles was named ODA-GO.

To functionalize GO, the silane agents were dissolved in a 200 ml mixture of water/methanol at a ratio of 75:25, then 2 g of the ODA-GO was added to the vessel and the suspension was stirred during 5 h at $80 \text{ }^\circ\text{C}$. The functionalized particles were filtered, washed subsequently with methanol, then with 50:50 water/methanol mixtures for at least three times to remove any unreacted silanes. Finally, the modified particles were dried in a vacuum oven at $105 \text{ }^\circ\text{C}$ for 24 h, then ground, pulverized and stored for further use. The functionalized GOs prepared from the silanes were denoted as AMPTES-GO and GPTMS-GO.

Preparation of functionalized polypropylene

The modification reaction was carried out in the molten state by using a 50 ml Brabender PL2100 mixer. PP, 2 wt% of MAH, and 0.1 wt% of DCP were introduced in the preheated mixer at $180 \text{ }^\circ\text{C}$ and mechanically mixed at 30 rpm for 10 min. The product was granulated and kept firmly away from the humidity in plastic bags. The grafting fraction was determined by titration of the acid groups from the anhydride functions according to the previously reported procedure [22]. The grafting fraction was found to be 1 wt% of maleic anhydride groups.

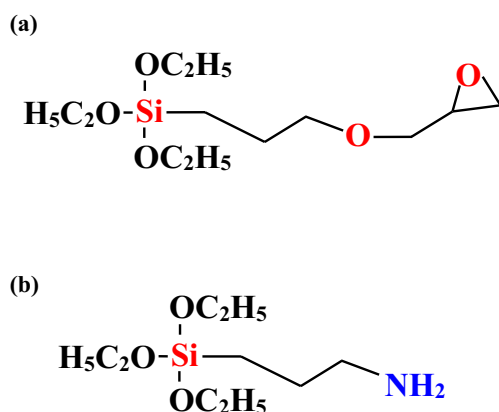


Fig. 1 Chemical formulas of silane coupling agents (a) GPTMS and (b) AMPTES

The amine and alcohol functionalized polypropylene were prepared by the reaction of PP-g-MAH with 1,12-dodecanediamine and 1,12-dodecanediol, respectively. First, the PP-g-MAH was melted in a Brabender mixer for 3 min at 190 °C and 40 rpm, then 2 wt% of the diamine or dialcohol was added. After mixing for another 7 min, samples were removed from the Brabender, solidified and grinded into pellets. The obtained material was dissolved and purified in xylene for 24 h in order to remove any remaining diamine or dialcohol. Finally, the product was dried in vacuum at 60 °C to constant weight. The functionalized PP prepared from diamine and dialcohol were denoted as PP-g-NH₂ and PP-g-OH, respectively.

Elaboration of nanocomposites

The various formulations and their respective designations used in this study are shown in Table 2. Nanocomposites were prepared in a two-step compounding process. First, a predispersed GO and functionalized GO masterbatches were prepared using a Brabender mixer at 190 °C and a rotor speed of 30 rpm. The masterbatches were then incorporated into PP/EPR matrix in a 95/5 proportion and allowed to mix for 8 min at 200 °C and 60 rpm in the Brabender PL2100 mixer. The resulting PP/EPR/GO nanocomposite is hence composed of 1 wt% GO and 15 wt% of compatibilizers (PP-g-NH₂ and PP-g-OH). After pelletizing, the composite granules were compression molded using a hydraulic press at 200 °C and 200 Kg/cm² for 6 min.

Characterization

ATR-FTIR spectroscopy was used to confirm the formation and functionalization of GO. About 50 mg of the GO were compacted into thin pellets using a hydraulic press under a

force of 5 tons maintained for about 4 min. Samples were analyzed by signal averaging 16 scans at a resolution of 4 cm⁻¹ using a JASCO-IR spectrometer. FTIR analysis was also performed to confirm the grafting reaction of MAH, amine and alcohol onto PP. Thin films were obtained from the samples by compression molding between two Teflon sheets using a compression machine at 200 °C and 180 kg/cm². The spectra were recorded on a Shimadzu spectrometer in a transmission mode at 4 cm⁻¹ with the coaddition of 32 scans with a spectral range of 4000–400 cm⁻¹.

XRD analyses of the GOs samples were performed using a BRUCKER D8 Advance diffractometer. The radiation frequency used was the K α_1 line from Cu (1.54 Å), with a power supply of 40 kV and 40 mA. The interlaminar distances of the sheets were obtained from the (002) reflection which were recorded in the 2-theta (2 θ) range from 5 to 40° at steps of 0.01° and intervals of 6 s per step, using Bragg's eq. [23].

Mechanical properties of the nanocomposites were evaluated by tensile and impact strength measurements. Tensile properties were measured using an Instron MTC 500 machine at a cross head speed of 20 mm/min. The tensile strength, Young's modulus and elongation at yield and break were determined from the stress-strain curves according to ASTM D 638 specifications. Impact testing was carried out using a Ceat impact pendulum tester with an impact energy of 7.5 KJ according to ASTM D 256–88. The hammer velocity was set at 2.88 m/s while the weight of the hammer was 1.8 Kg. All measurements were made in five replicants and the values were averaged.

The morphology of the nanocomposites was analysed using with a Quanta 200 Scanning Electron Microscope at an acceleration voltage of 10 kV. Test specimens, produced by compression molding at 200 °C and 180 Kg/cm², were

Table 2 Composition and designation of Polymer/GO nanocomposites

Formulations	(PP/EPR) (%)	PP-g-NH ₂ (%)	PP-g-OH (%)	GO (%)	GPTMS-GO (%)	AMPTES-GO (%)	Designation
PP	100	0	0	0	0	0	F0
PP/EPR	100	0	0	0	0	0	F1
PP/EPR/PP-g-NH ₂	85	15	0	0	0	0	F2
PP/EPR/PP-g-OH	85	0	15	0	0	0	F3
PP/EPR/GO	99	0	0	1	0	0	F4
	99	0	0	0	1	0	F5
	99	0	0	0	0	1	F6
PP/EPR/PP-g-NH ₂ /GO	84	15	0	1	0	0	F7
	84	15	0	0	1	0	F8
	84	15	0	0	0	1	F9
PP/EPR/PP-g-OH/GO	84	0	15	1	0	0	F10
	84	0	15	0	1	0	F11
	84	0	15	0	0	1	F12

frozen by immersion in liquid nitrogen to obtain brittle fractured specimen.

TGA of both GOs and polymer nanocomposite samples was conducted using a Setaram SETSYS TG-DTA thermal analyser under nitrogen atmosphere at a flow rate of 20 ml/min. About 10 to 20 mg of each sample was heated from 30 to 500 °C with a heating rate of 10 °C/min.

Results and discussion

In order to prove the formation of GO, ATR-FTIR measurement was conducted. Figure 2 shows the FTIR results of pristine graphite, purified graphite and graphene oxide. While no absorption bands observed suggests the functional groups in pristine graphite (Fig. 2a), purified graphite (Fig. 2b, c) and graphene oxide (Fig. 2d) was found to exhibit several characteristic absorption bands of oxygen-containing groups (Fig. 2b, c). The broad band at 3604–3285 cm^{-1} is characteristic of the stretching vibration of the O-H and -COOH groups. The intense band at 1729 cm^{-1} is attributed to the -C = O stretching of -COOH group. The bands located at 1623 cm^{-1} and 1371 cm^{-1} may refer to the stretching of the C = O bond of carbonyl groups and O-H bond of alcohol functions, respectively. The absorption band at 1580 cm^{-1} is attributed to skeletal vibrations of unoxidized graphitic domains. The band at 900 cm^{-1} corresponds to the aromatic C-H bonds. The bands present at 1221 cm^{-1} and 1059 cm^{-1} are attributed to the presence of ethers, phenols and epoxy functions. This shows that the purification treatments of the graphite also create oxygenated functions even

on the surface of mineral. The low intensity bands at 2913 and 2845 cm^{-1} were attributed to the stretching vibration of the aliphatic sp^3 , C-H, which prove the oxidation process.

The XRD patterns of purified graphite and GO as well as that of raw graphite are shown in Fig. 3. The pattern of the raw graphite shows a very strong (002) peak at $2\theta = 26.5^\circ$, for a typical graphitic structure with a layer spacing of 0.345 nm. However, after purification, it is obvious that the characteristic graphitic peak completely disappears and a new diffraction peak appears at about $2\theta = 24^\circ$ with a layer spacing of 0.385 nm. This slight increase is attributed to the formation of oxygenated groups and to the intercalation of water molecules within carbon layer structure. These results are in good agreement with those obtained by FTIR spectroscopy.

In the case of GO, the peak corresponding to (002) plane of graphite vanishes with the appearance of a new peak at around $2\theta = 15.2^\circ$, which corresponds to a (001) plane. The average d-spacing between the graphene planes is observed at 0.583 nm.

TGA is a complementary technique that can reveal the composition and changes in thermal stability of the samples. TGA analyses of pristine graphite, purified graphite and GO are illustrated in Fig. 4. It is observed that the pristine graphite is highly stable up to 500 °C. The thermal degradation profile for the purified graphite exhibits one weight loss step at 250 °C. The TGA curve obtained for GO sample shows two weight loss steps around 100 °C and 250 °C. The former is due to the release of physisorbed water molecules and the decomposition of the labile oxygen-containing functional groups such as -COOH, -OH and -C = O groups, yielding CO, CO₂, and steam [24].

Fig. 2 ATR-FTIR spectra of (a) pristine graphite, (b) purified graphite by oxidative treatment in air (c) purified graphite by oxidative treatment in solution and (d) Graphene oxide

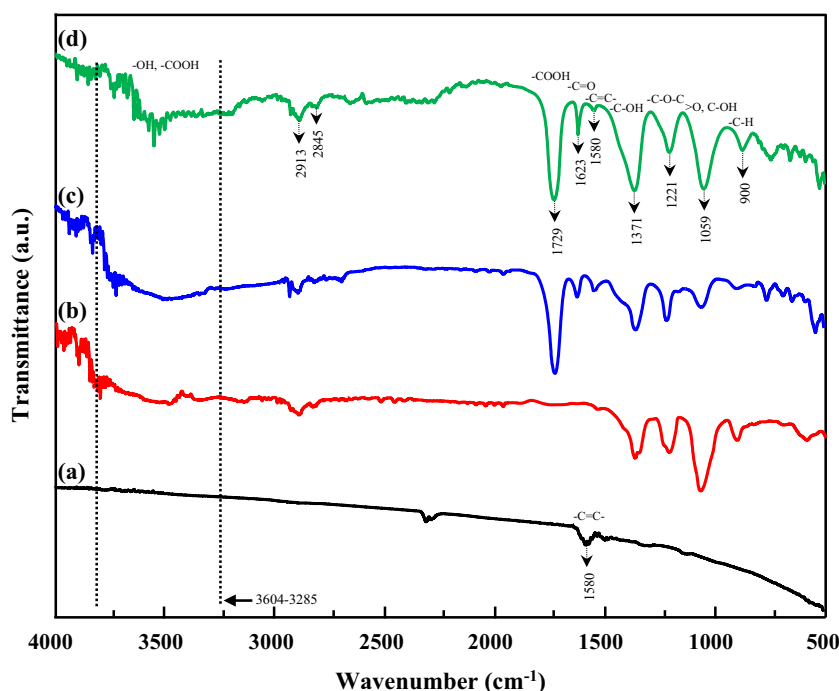


Fig. 3 XRD patterns of (a) pristine graphite, (b) purified graphite and (c) graphene oxide

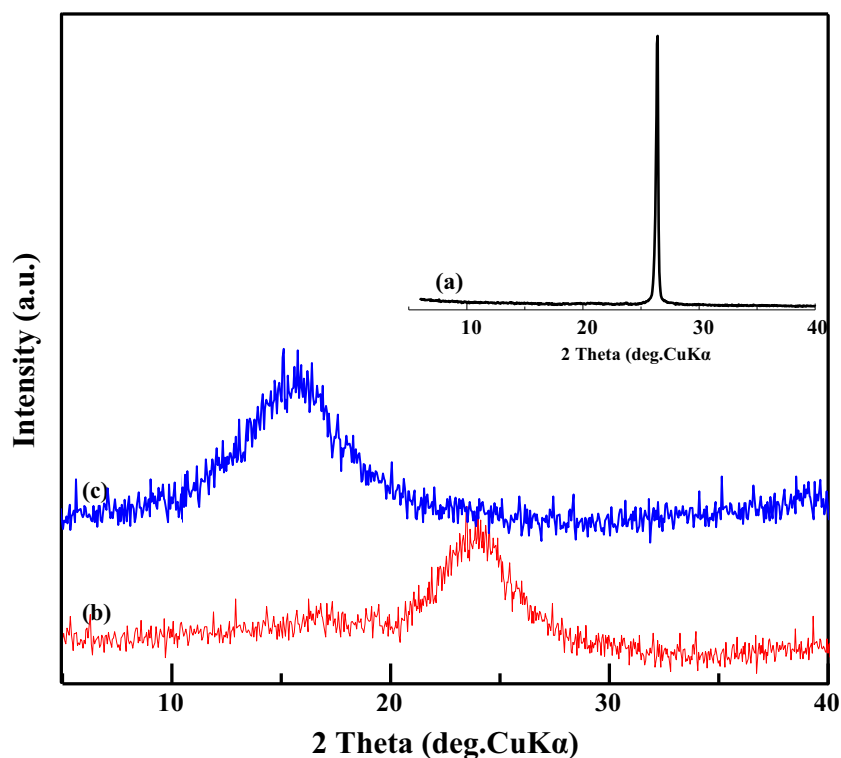


Figure 5 shows the FTIR spectra of ODA-GO in comparison to pure HDA and GO spectra. The spectrum of ODA-GO (Fig. 4c) exhibits two strong bands at 2925 cm^{-1} and 2850 cm^{-1} which correspond to -CH asymmetric and symmetric stretching of $-\text{CH}_2$ groups in ODA. This confirms its successful grafting on GO surface.

The bands appearing at 3455 cm^{-1} and 3236 cm^{-1} are assigned to the vibration of the NH-CO, which means that the ODA interacts onto the surface with the -COOH functional

groups of GO. The band related to the $-\text{C}=\text{O}$ stretching of -COOH groups appearing at 1729 cm^{-1} in the spectrum of GO shifts to 1690 cm^{-1} with a decrease in the band intensity and reveals the formation of CO-NH linkage in the surface of GO. The bands at 1530 cm^{-1} and 1055 cm^{-1} are attributed to the vibration of N-H and C-N bonds corresponding to the secondary amide.

Figure 6 presents the FTIR spectra of GPTMS-GO in comparison to the reference spectra, which are those of the pure

Fig. 4 TGA curves of (a) pristine graphite, (b) purified graphite and (c) graphene oxide

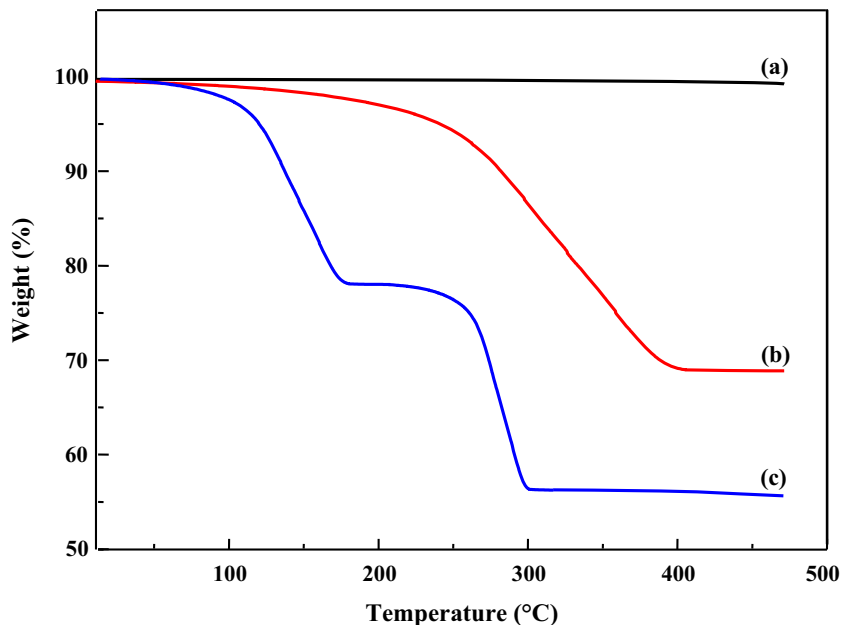
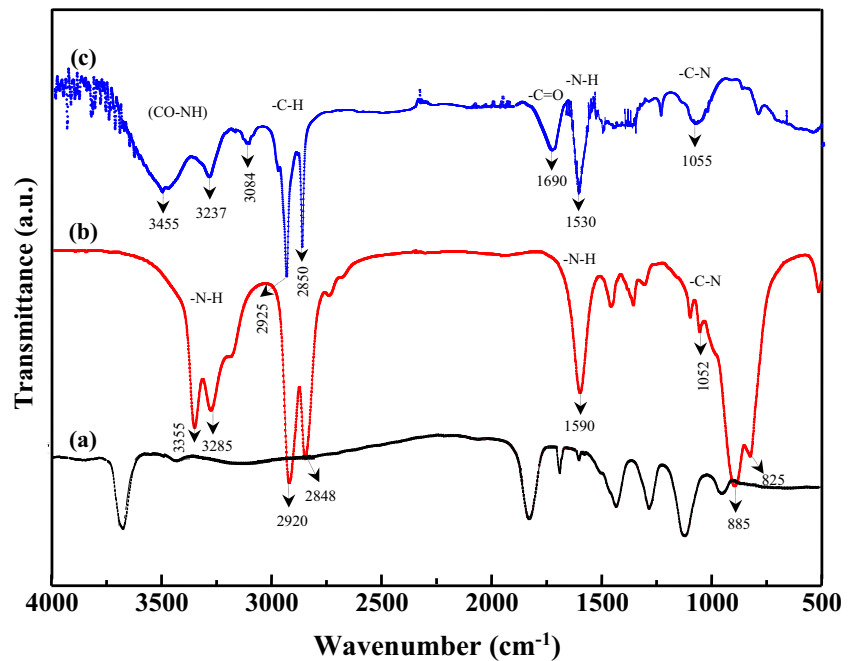


Fig. 5 ATR-FTIR spectra of (a) GO, (b) pure ODA and (c) ODA-GO



GPTMS and GO. In the GPTMS-GO spectrum (Fig. 5c), the broad band centered at 3655 cm^{-1} results from the -OH functional groups of Si-OH and water. The band positioned at 1640 m^{-1} is also attributed to the -OH bond of water. The strongest bands which appeared at 2940 cm^{-1} and 2838 cm^{-1} are attributed to the $\text{-CH}_2\text{-}$ groups of the GPTMS propyl segments. The absorption bands located at 1130 cm^{-1} and 1044 cm^{-1} are assigned to the siloxane bonds resulting from the condensation of silane molecules. The bands at 1455 cm^{-1} and 874 cm^{-1} are attributed to the $\text{-CH}_2\text{-}$ of the glycidoxy groups and the epoxy ring, respectively.

Fig. 6 ATR-FTIR spectra of (a) GO, (b) pure GPTMS and (c) GPTMS-GO

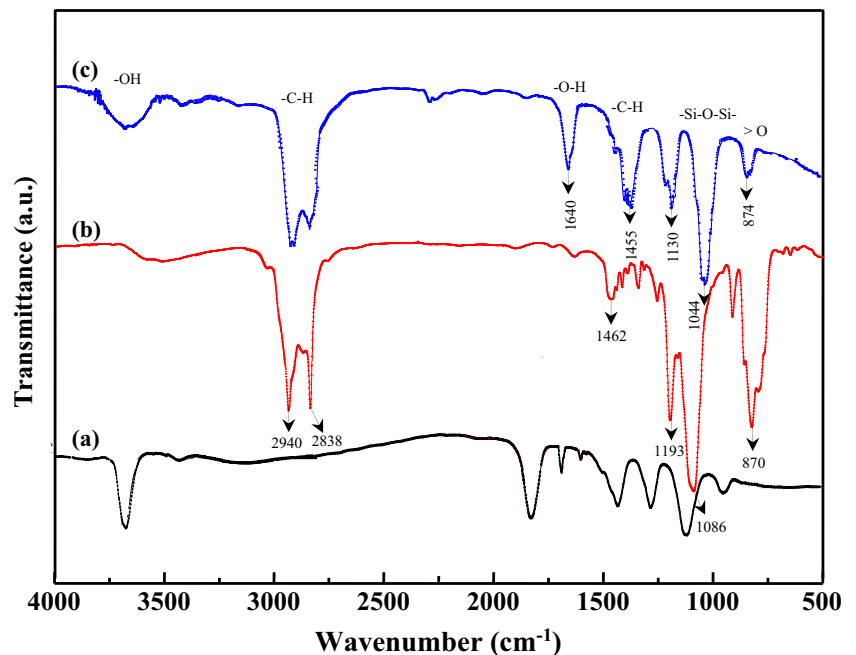
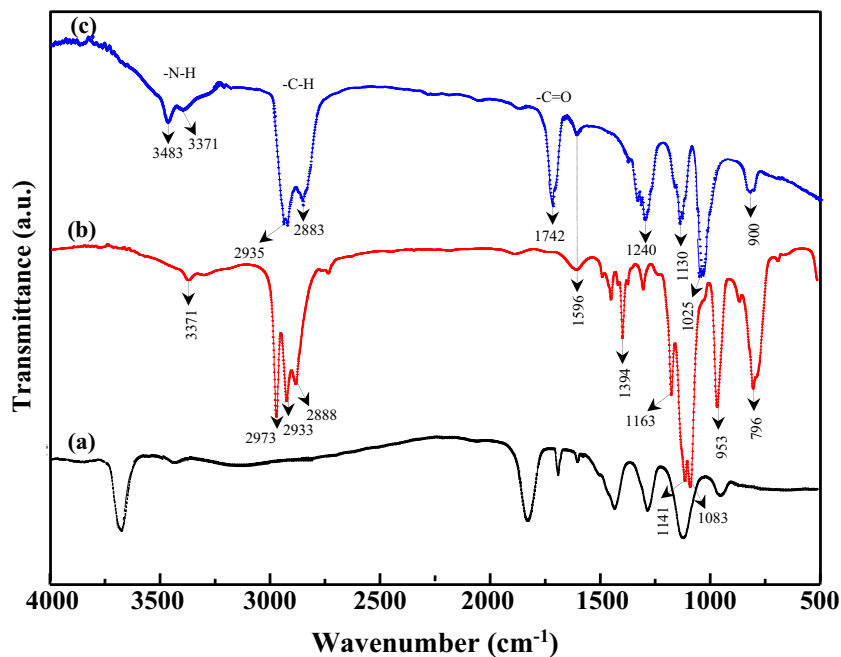


Figure 7 shows the FTIR spectra of AMPTES-GO, in comparison to the reference spectra, which are those of the pure AMPTES and GO. The spectrum of AMPTES-GO exhibits two intense bands at 2981 cm^{-1} and 2898 cm^{-1} which are attributed to the stretching vibrations of the C-H bonds of the methylene groups of the aminopropyl segment. The band positioned at 1742 cm^{-1} is assigned to the vibrations of the esters carbonyl group $\text{C}=\text{O}$. The bands located at 3483 cm^{-1} and 3371 cm^{-1} and the band positioned at 1596 cm^{-1} correspond to the N-H bond which are characteristics of primary amine functions. The bands centered at 1130 cm^{-1} and 1025 cm^{-1} are

Fig. 7 ATR-FTIR spectra of (a) GO, (b) pure AMPTES and (c) AMPTES-GO



characteristic of the siloxane bonds. This result suggests that the AMPTES reacts rather via the silanol functional groups with -COOH or -OH functional groups forming a polysiloxane network.

The successful grafting of GO with ODA, GPTMS and AMPTES is further corroborated with TGA results (Fig. 8). The loss observed at the temperature range 120–250 °C for HDA-GO sample, is attributed to the transformation of some oxygen-containing groups which react with HDA. Decomposition of the alkyl groups in ODA occurs between 300 °C and 460 °C.

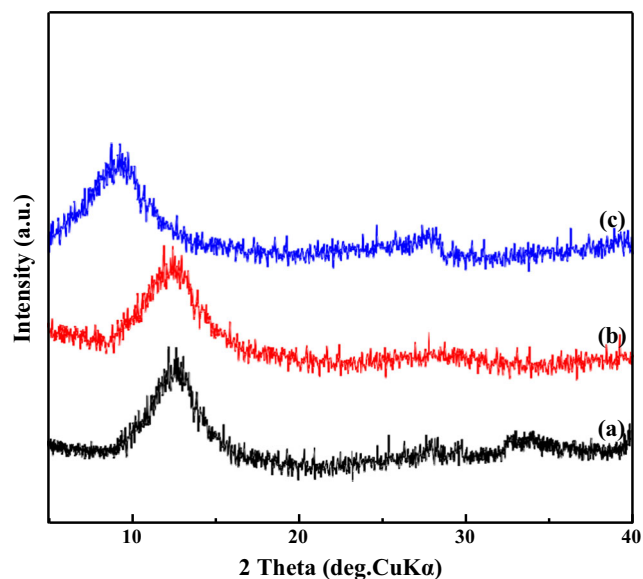


Fig. 8 XRD patterns of (a) HDA-GO, (b) GPTMS-GO and (c) AMPTES-GO

The thermal decomposition profiles for GPTMS-GO and AMPTES-GO exhibit one weight stage at 325 °C and 350 °C, respectively. This is due to the release of silane molecules. The higher combustion temperature of silylated materials in comparison with ODA-GO demonstrates the higher thermal stability of these samples because of the reduction of defects created during the formation of GO.

Figure 9 shows the X-ray diffraction patterns of HDA-GO, GPTMS-GO and AMPTES-GO samples. After intercalation of GO with HDA (Fig. 9a), the diffractogram shows a shift of 2θ angle to lower values. The peak position at $2\theta = 12.1^\circ$, corresponds to a layer spacing of 0.73 nm. The increase of the layer spacing is attributed to the intercalation of amine molecules within the structure of graphitic layer. After silanization of HDA-GO with GPTMS (Fig. 9b), the peak position does

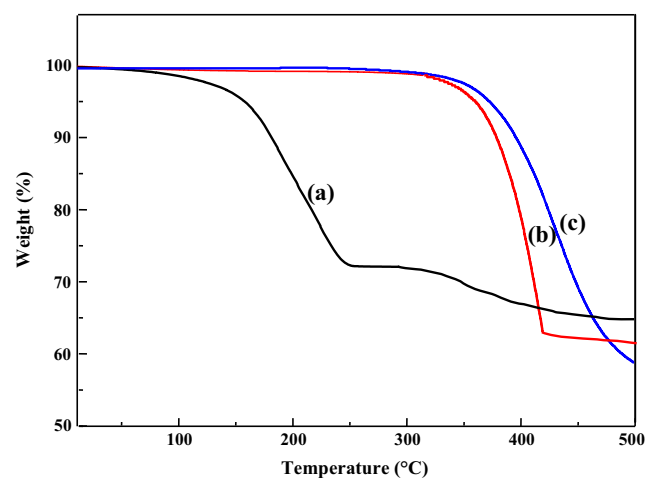
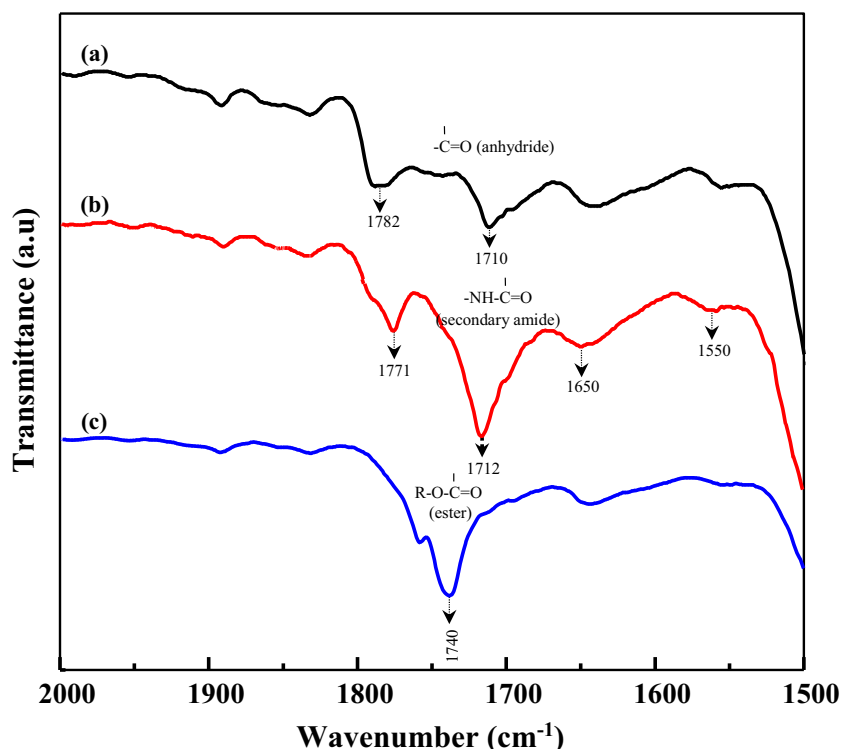


Fig. 9 TGA curves of (a) ODA-GO, (b) GPTMS-GO and (c) AMPTES-GO

Fig. 10 FTIR spectra in the range 2000–1500 cm^{-1} of (a) PP-g-MAH, (b) PP-g-NH₂ and (c) PP-g-OH



not change, which that suggests the interlayer space has not expanded. Also, silanization of HDA-GO with AMPTES (Fig. 9c) shifts to lower values. The peak position for the sample at $2\theta = 8.3^\circ$ value, corresponds to a layer spacing of 1.1 nm. This is explained by the ability of the aminosilane to be grafted on the internal surfaces of the graphene oxide and the polycondensation of these grafted molecules in a three-dimensional siloxane network.

The grafting of PP was also confirmed using ATR-FTIR spectroscopy. The FTIR spectra of PP-g-MAH, PP-g-NH₂ and PP-g-OH are shown in Fig. 10. The spectrum of PP-g-MAH (Fig. 10a) shows two bands at 1782 cm^{-1} and 1710 cm^{-1} , which are characteristic of cyclic anhydride groups. The spectrum of PP-g-NH₂ (Fig. 10b) displays four bands due to the formation of the imide groups. The band at 1771 cm^{-1} is assigned to the asymmetrical stretching of carbonyl groups in imide. The band at 1712 cm^{-1} is attributed to the stretching of carbonyl groups in carboxylic acid. The strong intensity of this band is attributed to the symmetrical stretching of the carbonyl groups in imide. The

two bands appearing at 1650 cm^{-1} and 1550 cm^{-1} correspond to the vibration of the secondary amide groups. The spectrum of PP-g-OH (Fig. 10c) shows one band at 1740 cm^{-1} which is characteristic of the ester carbonyl groups.

Mechanical properties of the nanocomposites

One of the major deficiencies of PP is its low stiffness at high temperature, as well as low impact resistance, especially at low temperature because of its relatively high glass transition temperature. An alternative was developed in order to improve the impact toughness of PP by adding both soft and rigid particles [25–27].

The tensile and Izod impact strength results of the different nanocomposites are presented in Table 3. As expected it is shown that the addition of EPR led to a substantial improvement in ductility. This was indicated by the elongation at break of PP which increased by 180%, whereas Young's modulus and tensile strength decreased by 92% and 44%, respectively. The Izod

Table 3 Tensile properties of neat PP, PP/EPR and compatibilized blends

Properties	Materials			
	PP	PP/EPR	PP/EPR/PP-g-NH ₂	PP/EPR/PP-g-OH
Tensile strength, σ_b (MPa)	36 ± 0.2	20 ± 0.3	19 ± 0.5	20 ± 0.4
Modulus, E (MPa)	1500 ± 23	1015 ± 25	1112 ± 21	1125 ± 27
Elongation at break, ϵ_b (%)	39 ± 12	109 ± 9	70 ± 14	78 ± 7
Impact strength, a_k (kJ/m ²)	4.6 ± 2	6.8 ± 1.4	6.2 ± 1	6.4 ± 1.6

Table 4 Tensile properties of PP/EPR/GO and compatibilized nanocomposites

Properties	Materials		
	PP/EPR/GO	PP/EPR/PP-g-NH ₂ /GO	PP/EPR/PP-g-OH/GO
Tensile strength, σ_b (MPa)	21.4 ± 0.1	23 ± 0.4	27 ± 0.2
Modulus, E (MPa)	1155 ± 20	1225 ± 25	1454 ± 23
Elongation at break, ε_b (%)	51.4 ± 7	49 ± 9	41 ± 5
Impact strength, a_k (kJ/m ²)	5.44 ± 1.8	5.4 ± 1.2	4.9 ± 1

impact strength increased from 4.6 kJ/m² up to 6.8 kJ/m², which corresponds to an increase of about 47% compared to neat PP. These results were generally observed in various blends and have been attributed to the softening or diluting influence of the addition of soft elastomeric particles to the polymeric matrix [28, 29].

Introducing the compatibilizers in PP/EPR blend increased slightly the modulus value, decreased the elongation at break while maintaining the impact strength constant. It is believed that the reduction of the elongation at break may result from a higher adhesion at the interface between the two phases, PP and EPR.

Table 4 presents the results of the tensile and Izod impact strength of the nanocomposites modified by the addition of GO and the compatibilizers. It was found that the incorporation of GO has improved the tensile strength and Young's modulus. Tensile strength and Young's modulus increased by about 7% and 14%, respectively. In addition, the elongation at break and impact strength (Fig. 12) decreased by about 50% and 20% respectively as compared to the unfilled blend. This can be explained by the lack of interfacial adhesion between the non-polar PP/EPR matrix and the polar layered GO.

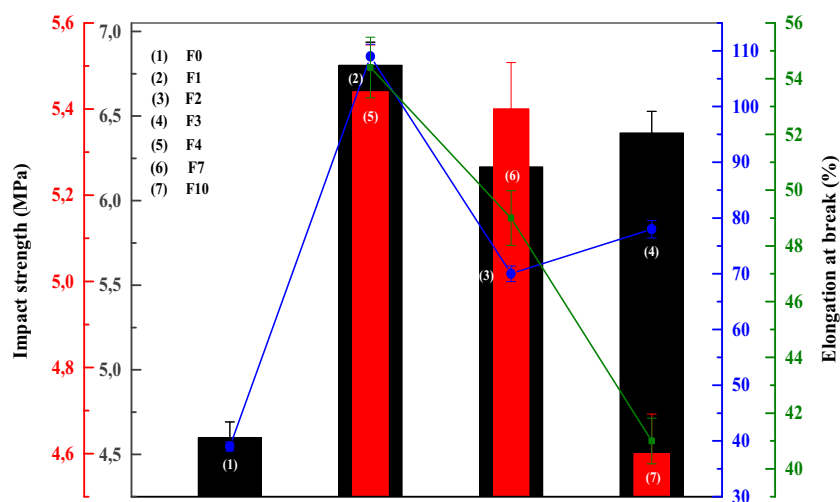
The addition of compatibilizers resulted in an improvement of the tensile strength and Young's modulus. It was also found that while the tensile strength and modulus of PP/EPR/PP-g-OH/GO increased by about 35% and 30% those of PP/EPR/PP-g-NH₂/GO increased by only 21% and 10%, respectively as compared to the unfilled blend. However, it is important to note that the PP-g-NH₂ compatibilized nanocomposites showed

higher elongation at break and impact strength as compared to PP-g-OH compatibilized nanocomposites (Fig. 11). It was also noted that the incorporation of compatibilizers into nanocomposites caused a slight increase of both elongation at break and Izod impact strength.

The improvement in the mechanical properties by the addition of compatibilizers; particularly PP-g-OH, results from greater adhesion at the interface between PP, EPR and GO. The interface would be the base of important interactions between the two phases due to the presence of the compatibilizer which concentrates preferentially at this level during the development of the blend phases.

It is noteworthy that the most important factor that can possibly contribute to the enhancement of the mechanical properties for materials with nanofillers is the dispersion and interaction of the polymer matrix with nanoparticles. Better dispersion of the filler within the matrix and a strong nanofiller-matrix interaction ensures effective load transfer between the components.

It is clear that the performance of a GO/polymer nanocomposite depends on the dispersion of GO in the matrix and interfacial interactions between the GO and the polymer matrix. However, several studies have not been able to provide consensus on the factors governing the nanofillers/matrix interface of composites. The functionalization of GO using non covalent and covalent methods can provide useful functional groups which make GO soluble in different organic solvents.

Fig. 11 Impact strength and elongation at break of (1) PP, (2) PP/EPR, (3) PP/EPR/PP-g-NH₂, (4) PP/EPR/PP-g-OH, (5) PP/EPR/GO, (6) PP/EPR/PP-g-NH₂/GO and (7) PP/EPR/PP-g-OH/GO

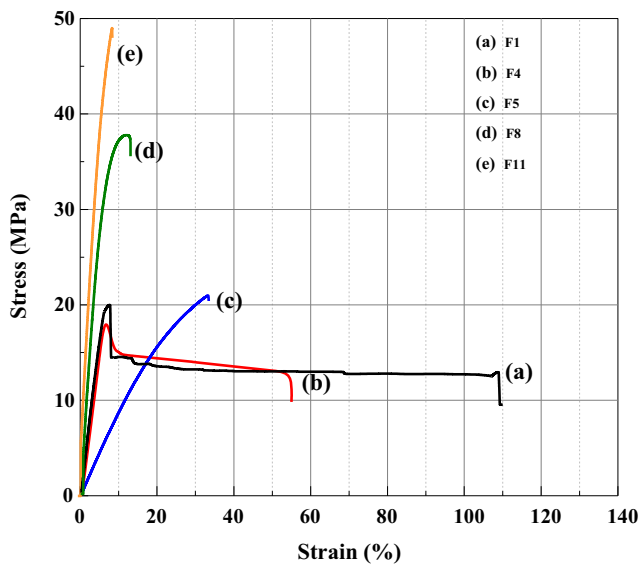


Fig. 12 Typical stress-strain curves of (a) PP/EPR, (b) PP/EPR/PP-g-OH, (c) PP/EPR/GO, (d) PP/EPR/PP-g-NH₂/GPTMS-GO and (e) PP/EPR/PP-g-OH/GPTMS-GO

As for the nanofillers-reinforced polymer composites, the load-deformation behaviour illustrates the intrinsic material properties. The efficiency of load transfer depends on the interfacial bonds between the filler and the polymer matrix.

Figure 12 depicts the typical stress-strain curves of the PP/EPR blend and its nanocomposites compatibilized with PP-g-OH and reinforced with pristine and functionalized GO. The detailed data of the mechanical tests of the materials are summarized in Table 5. It is observed that the incorporation of GO improves the tensile strength and the Young’s modulus; the reinforcement is more pronounced with the modified GO nanocomposites. Plastic deformation with necking was observed in only PP/EPR matrix and PP/EPR/GO. Yielding was observed at lower deformation for all compatibilized nanocomposites than for the non-compatibilized system. Such an evolution is evident and could be an indication that the rigid nanofiller phase was unable to deform and that an interfacial adhesion between the components of the nanocomposite took place.

The results showed that the functionalization of GO by means of GPTMS has improved the tensile strength from

18.6 MPa to 21 MPa which corresponds to an increase of about 12% for this non-compatibilized nanocomposite. In the case of the compatibilized nanocomposites the tensile strength showed an important improvement. For instance it increased by 82% for the PP/EPR/PP-g-OH/GPTMS-GO as compared to the same system without the coupling agents.

Similar improvements in Young’s modulus were also observed with all materials. The modulus values obtained for the compatibilized nanocomposites with PP-g-OH were greater than those for the other compositions. In these systems, the Young’s modulus increased by about 20% and 16% for the nanocomposites with GPTMS-GO and APTMS-GO, respectively compared to the nanocomposites without silane coupling agents. Several studies have attributed the reinforcement obtained in polymer-nanofiller hybrids to the restriction of mobility of the polymer chains as a result of strong interfacial interactions [30–33].

From Table 5 it can also be observed that the elongation at break and impact strength (Fig. 13) showed a decrease for all the nanocomposite systems with coupling agents compared to those without coupling agents. The lowest elongation at break and impact strength were observed with the compatibilized nanocomposites with PP-g-OH. The elongation at break and impact strength of PP/EPR/PP-g-OH/GPTMS-GO decreased by about 78% and 30%, respectively compared to the nanocomposites without coupling agents. The reason for this behaviour can be explained by the improvement of the interactions between the polymer matrix and GO particles owing to the compatibilizers and the silane coupling agent’s action. The glycidoxy and amino groups anchored on GPTMS-GO and AMPTES-GO surface were expected to react with the functional groups of the compatibilizers, resulting in an improved compatibility of the GO with the polymer matrix.

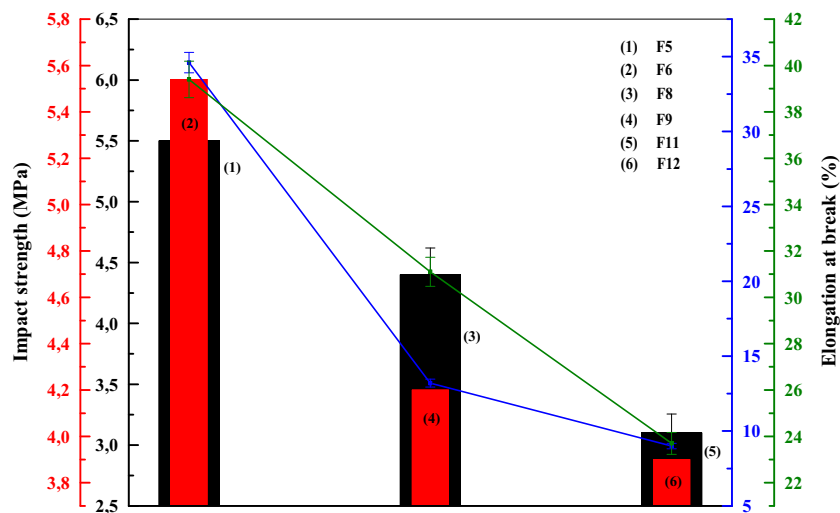
Thermogravimetric analysis of the nanocomposites

Figure 14 illustrates the thermogravimetric analysis of neat PP, blends and nanocomposites with and without the compatibilizers and coupling agents. It can be seen that the addition of the compatibilizer does not induce any significant variation in terms of decomposition in comparison with the

Table 5 Tensile properties of PP/EPR/GO and compatibilized nanocomposites with and without coupling agents

Properties	Materials					
	PP/EPR/GO		PP/EPR/PP-g-NH ₂ /GO		PP/EPR/PP-g-OH/GO	
	GPTMS	AMPTES	GPTMS	AMPTES	GPTMS	AMPTES
Tensile strength, σ_b (MPa)	18.8 ± 0.2	16.3 ± 0.5	37 ± 0.5	33 ± 0.2	49.2 ± 0.1	42.6 ± 0.4
Modulus, E (MPa)	879.4 ± 10	875.7 ± 12	1315 ± 15	1283 ± 20	1740 ± 12	1679 ± 10
Elongation at break, ϵ_b (%)	34.6 ± 6	39.4 ± 3	13.2 ± 6	31.1 ± 8	9 ± 3	23.7 ± 4
Impact strength, a_k (kJ/m ²)	5.5 ± 1.8	5.54 ± 1.1	4.4 ± 1	4.2 ± 1.2	3.1 ± 1.6	3.9 ± 1.1

Fig. 13 Impact strength and elongation at break of (1) PP/EPR/GPTMS-GO, (2) PP/EPR/APTMS-GO, (3) PP/EPR/PP-g-NH₂/GPTMS-GO, (4) PP/EPR/PP-g-NH₂/AMPTES-GO, (5) PP/EPR/PP-g-OH/GPTMS-GO and (6) PP/EPR/PP-g-OH/AMPTES-GO



neat matrix. This result is well illustrated with two temperatures characterizing these thermograms. The first of which is the temperature of the onset decomposition (T_{onset}) that takes place at 360 °C. The second is the one that marks the constant weight reached that corresponds to the maximum temperature of decomposition (T_{max}) around 455 °C.

For PP/EPR/GO sample, the T_{onset} and T_{max} shifted towards higher temperatures, indicating that the addition of GO can improve the thermal stability significantly. The results show that the T_{onset} and T_{max} of PP/EPR/GO sample are 400 °C and 465 °C, respectively corresponding to an increase by 40 °C and 10 °C, respectively, compared to the neat matrix. The process of the decomposition in PP/EPR/GPTMS-GO sample and for all other materials containing compatibilizers and silane coupling agents exhibited a similar behaviour. The

T_{onset} and T_{max} shifted to 430 °C and 490 °C, respectively with an increase of 40 °C and 35 °C respectively, compared to the neat matrix. The improved thermal stability is due to the barrier effect of GO particles against volatile gases formed during thermal degradation. This effect is amplified in the presence of the compatibilizers and coupling agents. This may be attributed to a uniform dispersion and distribution of the GO particles throughout the matrix. It may also be attributed to an adsorption effect at the filler surface of the released gases which slowed down the polymer decomposition. Similar results were obtained for the polymer/nanoclay and polymer/CaCO₃ composites [34, 35]. The reason of the improvement of the thermal stability can also be attributed to the better adhesion between polymer the matrix and GO particles owing to the compatibilizer and silane coupling agent's effects.

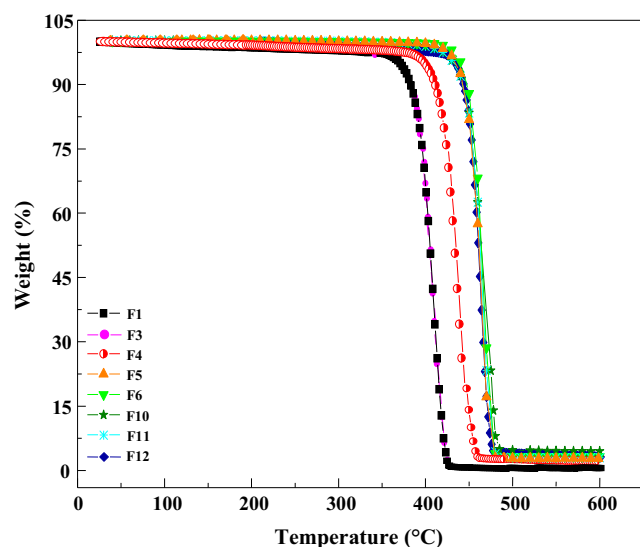


Fig. 14 TGA curves of —■— PP/EPR, —●— PP/EPR/PP-g-OH, —○— PP/EPR/GO, —▲— PP/EPR/GPTMS-GO, —▼— PP/EPR/AMPTES-GO, —★— PP/EPR/PP-g-OH/GO, —✱— PP/EPR/PP-g-OH/GPTMS-GO and —◆— xPP/EPR/PP-g-OH/AMPTES-GO

SEM analysis of the nanocomposites

Figure 15 shows the SEM photomicrographs of neat PP, PP/EPR and PP/EPR/PP-g-OH blends. Figure 15a shows that the PP exhibits a brittle fracture since the surface was rather smooth. The SEM photomicrograph of PP/EPR blend (Fig. 15b) clearly shows the formation of a two phase matrix-particle microstructure. The blending of PP with EPR lead to two immiscible systems where the minor phase of the elastomer disperses as spherical particles throughout PP. Several studies of PP/Elastomer blends report a phase separation between PP and EPR phases, well obviously when PP is a major phase [36–38]. In addition, the voids observed in the PP/EPR blend are believed to be due to the elastomeric particles dislodged from the fractured surface, reflecting a poor adhesion with the matrix. Similar morphology was observed in PP/EPR/PP-g-OH blend, but with a finer dispersion of the elastomeric particles in the matrix.

The SEM photomicrographs of nanocomposites are illustrated in Fig. 16. Agglomeration of particles can be seen when

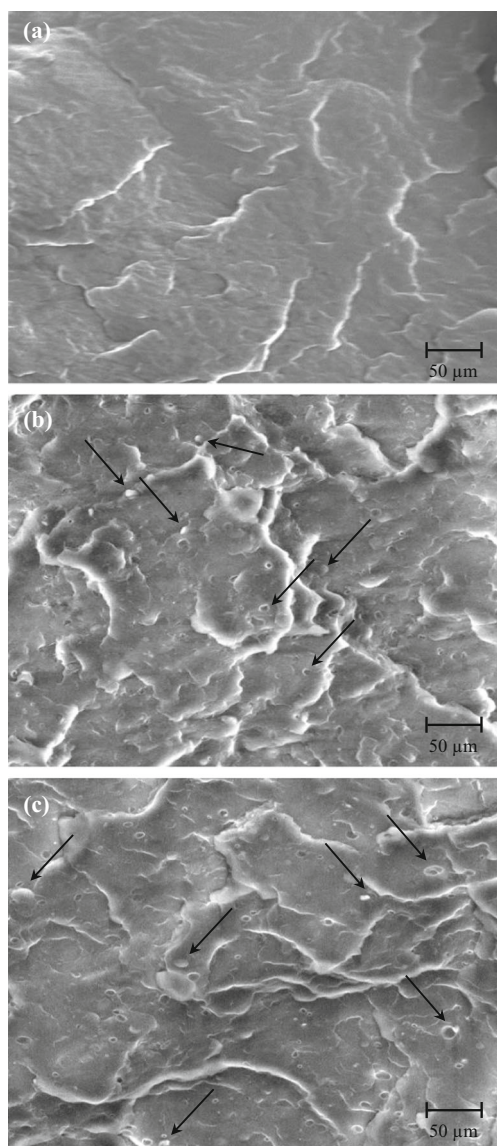


Fig. 15 SEM images of (a) PP, (b) PP/EPR and (c) PP/EPR/PP-g-OH

the unmodified GO was incorporated in the matrix (Fig. 16a). This phenomenon is visibly reduced when the modified GO with the silane coupling agents was incorporated (Fig. 16b and Fig. 16c). However, a better dispersion of GO particles was observed with the incorporation of silane modified GO, due to the reduction of the surface of the attraction forces between the particles.

Conclusions

Blends of polypropylene (PP) and ethylene-propylene rubber (EPR) were investigated to determine the influence of GO and its derivatives on the mechanical, thermal and morphological properties. The compatibilization effects imparted by amine and alcohol grafted polypropylene for PP/EPR

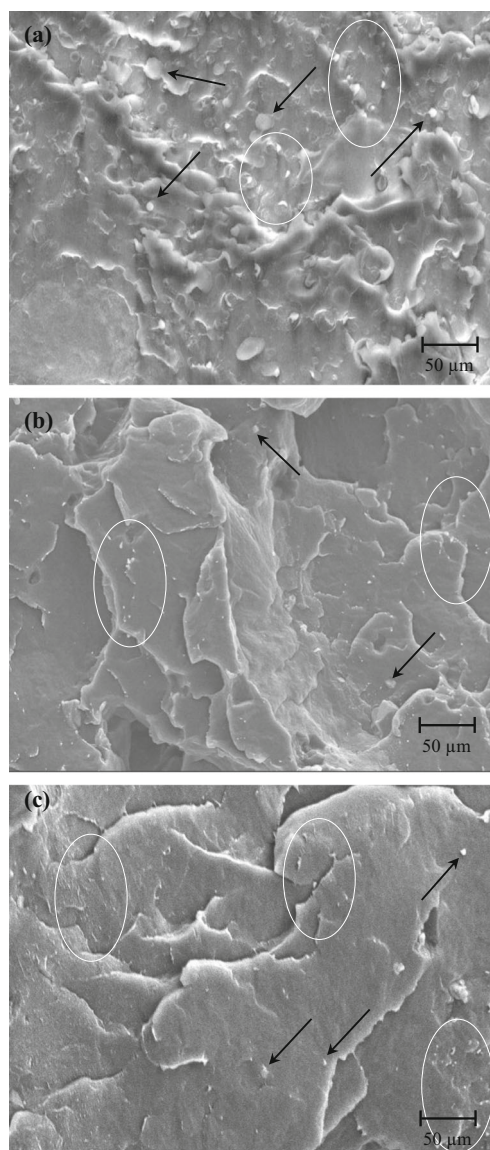


Fig. 16 SEM images of (a) PP/EPR/PP-g-OH/GO, (b) PP/EPR/PP-g-OH/GPTMS-GO and (c) PP/EPR/PP-g-OH/AMPTES-GO nanocomposites

nanocomposites were also investigated. Amine and alcohol functionalized polypropylene systems were elaborated using maleic anhydride functionalized polypropylene with 1,12-dodecanediamine and 1,12-dodecanediol in the presence of dicumyl peroxide (DCP). A significant improvement of the tensile strength and Young's modulus was observed when GO was incorporated in the matrix. The reinforcing effect was more pronounced for compatibilized nanocomposites and functionalized GO. In these nanocomposites higher strength and modulus were subsequently accompanied by a decrease in the elongation at break and impact strength. This was explained as the consequence of the enhancement of the adhesion at the interface due to a better dispersion of functionalized GO and chemical bonding between organofunctional groups in GO and the functionalized polypropylene. The thermal

behaviour determined by TGA showed a higher thermal stability for nanocomposites with functionalized GO in comparison with pristine GO. It was also found that the compatibilized nanocomposites exhibited the highest thermal stability compared to the non compatibilized nanocomposites. SEM photomicrographs of the fractured surfaces of the nanocomposites confirmed a good dispersion of the functionalized GO in the polymer matrix, resulting in an enhancement of the mechanical properties.

References

- Kroto HW, Heath JR, O'Brien SC, Curl RF, Smalley RE (1985) C₆₀: Buckminsterfullerene *Nature* 318:162–163
- Iijima S (1991) Helical microtubules of graphitic carbon *Nature* 354:56–58
- Galpaya D, Wang M, Liu M, Motta N, Waclawik E, Ya C (2012) Recent advances in fabrication and characterization of graphene-polymer nanocomposites *Graphene* 1:30–49
- Viculis LM, Mack JJ, Mayer OM, Hahn HT, Kaner R (2005) Intercalation and exfoliation routes to graphite nanoplatelets *J Mater Chem* 15(9):974–978
- Cui Y, Kundalwal SI, Kumar S (2016) Gas barrier performance of graphene/polymer nanocomposites *Carbon* 98:313–333
- Lerf A, He H, Forster M, Klinowski J (1998) Structure of graphite oxide revisited *J Phys Chem B* 102(23):4477–4482
- He H, Klinowski J, Forster M, Lerf A (1998) A new structural model for graphite oxide *Chem Phys Lett* 287(1–2):53–56
- Bhawal P, Ganguly S, Chakia TK, Das NC (2016) Synthesis and characterization of graphene oxide filled ethylene methyl acrylate hybrid nanocomposites *RSC Adv* 6(25):20781–20790
- Stankovich S, Dikin DA, Dommett GHB, Kohlhaas KM, Zimney EJ, Stach EA, Piner RD, Nguyen ST, Ruoff RD (2006) Graphene-based composite materials *Nature* 442:282–286
- Alireza A, Hossein R, Reza B (2015) Preparation and characterization of functionalized graphene oxide/carbon fiber/epoxy nanocomposites *Polym Test* 48:82–88
- Yang H, Li F, Shan C, Han D, Zhang Q, Niu L, Ivaska A (2009) Covalent functionalization of chemically converted graphene sheets via silane and its reinforcement *Mater Chem* 19(26):4632–4638
- Yuan B, Bao C, Song L, Hong N, Liew KM, Hu Y (2014) Preparation of functionalized graphene oxide/polypropylene nanocomposite with significantly improved thermal stability and studies on the crystallization behavior and mechanical properties *Chem Eng J* 237:411–420
- Ren PG, Wang H, Huang HD, Yan DX, Li ZM (2014) Characterization and performance of dodecyl amine functionalized graphene oxide and dodecyl amine functionalized graphene/high-density polyethylene nanocomposites: a comparative study *J Appl Polym Sci* 131(2):39803–39812
- Tripathi SN, Srinivasa Rao GS, Mathur AB, Jasra R (2017) Polyolefin/graphene nanocomposites: a review *RSC Adv* 38(7):23615–23632
- Hu W, Zhan J, Wang X, Hong N, Wang B, Song L, Stec AA, Hull TR, Wang J (2014) Effect of functionalized GO with hyperbranched flame retardant on flammability and thermal stability of cross-linked PE *Ind Eng Chem Res* 53(8):3073–3083
- Steurer P, Wissert R, Thomann R, Mulhaupt R (2009) Functionalized graphenes and thermoplastic nanocomposites based upon expanded graphite oxide *Macromol Rapid Commun* 30(4–5):316–327
- Chen Y, Qi Y, Tai Z, Yan X, Zhu F, Xue Q (2012) Preparation, mechanical properties and biocompatibility of graphene oxide/ultrahigh molecular weight polyethylene composites *Eur Polym J* 48(6):1026–1033
- Aizenshtein EM (2008) Polypropylene fibers and yarns in the current state of development *Fiber Chem* 40(5):399–405
- Stumberger N, Gospocic A, Bratulic C (2005) Polymeric materials in automobiles *Promet Traffic Traffico* 17(3):149–160
- Mehta S, Mirabella FM, Rufener K, Bafna A (2004) Thermoplastic olefin/clay nanocomposites: morphology and mechanical properties *J Appl Polym Sci* 92(2):928–936
- Lim JW, Hassan A, Rahmat AR, Wahit MU (2006) Rubber-toughened polypropylene nanocomposite: effect of polyethylene octene copolymer on mechanical properties and phase morphology *J Appl Polym Sci* 99(6):3441–3450
- Sánchez-Valdes S, Zapata-Domínguez AG, Martínez-Colunga JG, Méndez-Nonell J, Ramos de Valle LF, Espinoza-Martínez AB, Morales-Cepeda A, Lozano-Ramírez T, Lafleur PG, Ramírez-Vargas E (2016) Influence of functionalized polypropylene on polypropylene/graphene oxide nanocomposite properties. *Polym Compos* <http://www.chemurope.com>. Accessed 12 Oct 2016
- David IF, Shankland K, McCusker LB, Baerlocher C (2002) Structure determination from powder diffraction data. Oxford University Press Inc, New York,
- Stankovich S, Dikin DA, Piner RD, Kohlhaas KA, Kleinhammes A, Jia Y, Ruoff SBT (2007) Synthesis of graphene-based nanosheets via chemical reduction of exfoliated graphite oxide *Carbon* 45:1558–1565
- Hidayah IN, Mariatti M, Ismail H, Kamarol M (2015) Evaluation of PP/EPDM nanocomposites filled with SiO₂, TiO₂ and ZnO nanofillers as thermoplastic elastomeric insulators *Plast Rub Compos: Macromol Eng* 44(7):259–264
- Hamzah MS, Jaafar M, Mohd Jamil MK (2014) Electrical insulation characteristics of alumina, titania, and organoclay nanoparticles filled PP/EPDM nanocomposites *J Appl Polym Sci* 131(23):41184–41184
- Ranel AV, Abitha VK (2015) Study of mechanical, thermal and micro structural properties of EPDM/polypropylene/Nanoclay composites with variable compatibilizer dosage *J Mater Environ Sci* 6(1):60–69
- Tam WY, Cheung T (1996) Li RKY (1996) an investigation on the impact fracture characteristics of EPR toughened polypropylene *Polym Test* 15(4):363–379
- Van der Wal A, Nijhof R, Gaymans RJ (1999) Polypropylene-rubber blends: 2 the effect of the rubber content on the deformation and impact behaviour *Polymer* 40(22):6031–6044
- Doufnoune R, Haddaoui N, Riahi F (2006) Elaboration and characterization of an organic/inorganic hybrid material: effect of the interface on the mechanical and thermal behavior of PP/CaCO₃ composites *Int J Polym Mater* 55(10):815–834
- Doufnoune R (2005) Contribution à l'étude du comportement des mélanges Polymères/charges en présence d'agents de couplage. Ph.D thesis, Université Ferhat-ABBAS, Sétif, Algeria
- Hanemann T, Vinga Szabó D (2010) Polymer-nanoparticle composites: from synthesis to modern applications *Materials* 3:3468–3517
- Layek RK, Nandi AK (2013) A review on synthesis and properties of polymer functionalized graphene *Polymer* 54(19):5087–5103
- Frounchi M, Dadbin S, Salehpour Z, Nofereesti M (2006) Gas barrier properties of PP/EPDM blend nanocomposites *J Membrane Sci* 282:142–148
- Doufnoune R, Haddaoui N, Riahi F (2008) The effects of coupling agents on the mechanical, rheological and thermal properties of

- calcium carbonate-filled LDPE compatibilized with maleic anhydride-g-LDPE (part II) *Int J Polym Mater* 57(7):690–708
36. Gong L, Yin B, Li LP, Yang MB (2012) Morphology and properties of PP/EPDM binary blends and PP/EPDM/nano-CaCO₃ ternary blends *J Appl Polym Sci* 123(1):510–519
 37. Babu RR, Singha NK, Naskar K (2010) Interrelationships of morphology, thermal and mechanical properties in uncrosslinked and dynamically crosslinked PP/EOC and PP/EPDM blends *Express Polym Lett* 4(4):197–209
 38. Da Silva Ana Lúcia N, Rocha Marisa CG, Coutinho Fernanda MB, Rosário B, Scuracchio C (2000) Rheological, mechanical, thermal, and morphological properties of polypropylene/ethylene-octene copolymer blends *J Appl Polym Sci* 75(5):692–704